



# Assessment of tidal current potential in the Amapá's inner continental shelf (Eastern Amazonia - Brazil)

Robert Willian Queiroz Farias<sup>1</sup> · Maamar El -Robrini<sup>2</sup> · Osvaldo Ronald Saavedra<sup>3</sup>

Received: 29 November 2023 / Accepted: 11 August 2024 / Published online: 31 August 2024  
© Springer-Verlag GmbH Germany, part of Springer Nature 2024

## Abstract

This study addresses the global shift towards renewable energy due to the increasing demand driven by socioeconomic development. With finite fossil energy sources, there's a growing interest in oceanic renewable energy, estimated at 76 million MW. The Amazon, with its significant potential, particularly from predictable tidal currents in estuaries, stands out. The Inner Continental Shelf of Amapá, influenced by factors like water discharge ( $5,7 \times 10^{12} \text{ m}^3 \cdot \text{year}^{-1}$ ) and trade winds (speed:  $5\text{--}10 \text{ m} \cdot \text{s}^{-1}$ ) as well as Meso and Macrotidal, is a notable region. The paper focuses on hydrodynamic simulations considering different tidal scenarios and aims to assess the energy potential of tidal currents. Using the SisBaHiA two-dimensional hydrodynamic model, the study evaluates power density in key areas. The spring-neap cycle simulations identify promising zones in the Varador channel—upper section (tidal current velocity of  $1,53 \text{ m} \cdot \text{s}^{-1}$ –  $1.835 \text{ W} \cdot \text{m}^{-2}$ ) and lower section (tidal current velocity of  $1,12 \text{ m} \cdot \text{s}^{-1}$ –  $720,03 \text{ W} \cdot \text{m}^{-2}$ ). Notably, the upper Varador channel near the Inferno “igarapé” (Maraca Island) exhibits greater energy density, highlighting its potential in both spring and neap cycles. This research contributes valuable insights into the renewable energy potential of tidal currents in the Amapá region, supporting sustainable energy development.

**Keywords** ICSA · Hydrodynamic simulations · SisBaHiA · Tidal energy

## 1 Introduction

Replacing fossil fuel energy sources with clean renewable energy can be a way to avoid environmental and health impacts. Research into new energies from renewable sources and reducing the use of fossil fuels should favor the

energy transition. As renewable energy alternatives, there are solar, photovoltaic, biomass, wind, hydroelectric, geothermal and tidal (Chowdhury et al. 2021). In this context, sustainable energy development is important at a global level, since natural resources were once excessive and, over the years, have been decreasing. The possibility of capturing ocean energy, compared to traditional sources, has a high potential (Castello et al. 2020).

The maximum global tidal energy potential/year is around  $331\text{E}18$  Joules, while the theoretical potential is  $7,400\text{E}18$  Joules, so these results outweigh the total world consumption, confirming the relevance and exploring the trend of sustainable energy potential. If we only consider tidal energy, the oceanic potential in Brazil is above  $72 \text{ TWh} \cdot \text{year}^{-1}$  (Carneiro and Pentado Neto 2022). They are concentrated in three northern states of Brazil: Amapá, Pará and Maranhão (Neto et al. 2017). Specifically, the coast of the Amapá State has excellent energy indicators. Tide differences can reach 10 m in the Maracá island region.

For the characterization and decision-making of projects and sites with relevant energy potential, numerical approaches at different spatial and temporal scales are

Communicated by Ricardo de Camargo.

✉ Osvaldo Ronald Saavedra  
o.saavedra@ieec.org

Robert Willian Queiroz Farias  
robert.farias@itec.ufpa.br

Maamar El -Robrini  
robrini@ufpa.br

<sup>1</sup> Federal University of Pará, Technology Institute, Av. Augusto Correa 1, Belém 66075-110, Brazil

<sup>2</sup> Federal University of Pará, Naval Engineering and Oceanography Colleges, Av. Augusto Correa 1, Belém 66075-110, Brazil

<sup>3</sup> Electric Energy Institute, Federal University of Maranhão, Av. dos Portugueses, 1966, São Luís 65080-805, Brazil

fundamental for the initial phases of projects for harnessing tidal energy, as they allow for a deeper analysis of the study of the hydrodynamic model (Thiébot et al. 2020).

The application of numerical models in hydrodynamic studies is still recent and for this reason, scientific interest based on cutting-edge research in a numerical approach is of great value, as long as it has been used in a timely or comprehensive manner (Thiébot et al. 2020; Azevedo et al. 2023). Hydrodynamic modeling is a tool used in regional domains or river basins, such as the Amazon basin, to complement and provide a complete description of time and space of physical systems (Marta – Almeida 2022).

Some hydrodynamic modeling studies on renewable energy potential were developed in Amazon region: Numerical modeling of Maranhão Gulf tidal circulation and power density distribution (Czizewski et al. 2020); Hydraulic potential evaluation with hydrokinetic turbines for isolated systems in Amazon region locations (Oliveira et al. 2021b); Statistical relationship development for hydrokinetic energy potential assessment (Sood and Singal 2022); Energy potential and economic analysis of hydrokinetic turbines implementation in rivers: an approach using numerical predictions (CFD) and experimental data (Santos et al. 2019); Global riverine theoretical hydrokinetic resource assessment (Ridgill et al. 2021); Economic feasibility study of ocean wave electricity generation in Brazil (Oliveira et al. 2021b). This article aims to produce hydrodynamic simulations (mid-high tide, mid-low tide, high tide and low tide in spring and neap situations) and evaluate the energy density (tidal currents) of areas of interest in the Inner Continental Shelf of Amapá (ICSA).

This paper focuses on the energy characterization of the Maracá island area that seems to be a promising area for harnessing tidal currents to generate renewable energy. The relevance of this work lies in the fact that it includes this remote region as a potential producer of clean energy, which can promote the development of this area. As it is located on the equatorial margin and close to the ship routes that serve the large ports on the Amazon River, it presents attractive aspects for generating offshore green hydrogen for export. Maracá is an indigenous term meaning musical instrument (a hollow cylinder of light, thin wood filled with small stones and capped at the ends), a kind of rattle, used in festivals, religious ceremonies and warfare.

The relevance of this article lies in highlighting the renewable energy potential of this unique amazonian region. This potential can serve as a compelling argument against offshore oil exploration initiatives at the entrance of the vast Amazon estuary. Moreover, the study contributes to the discovery and understanding of a nearly unknown area characterized by the interaction between the ocean and the Amazon

River, emphasizing the importance of preserving its natural resources and focusing on sustainable development.

## 2 Study area location

The ICSA (2°11' and 1°50' N – 50°37' and 50°11' W) is adjacent to the Atlantic coast of Amapá, where the Varador channel separates the Maracá island, between the mouth of the Calçoene river estuary and Cabo Norte (Fig. 1). The ICSA (study area) can be described according to geomorphological features and the material type on the bottom of Amapá coastline to the depth limit delimited to the 10 m isobath.

## 3 Study area

### 3.1 Weather and meteorological parameters

According to Dubreuil et al. (2018), the study region is characterized by a warm monsoon type weather “Am”. The average annual air temperature follows a trend with a maximum in September and November months with 29 °C, and minimums in January to March months with 26 °C with super humid characteristics due to high rainfall and temperature range up to 3 °C. (INMET 2024; Lima et al. 2021). The Intertropical Convergence Zone (CZIT) is formed from the trade winds of the hemispheres that meet on the surface and cause moderate to heavy rainfall in Amapá. Also, its control over the tropical climate interferes with water and solid discharge.

The rainy season runs from November to March with high convective activity and heavy rainfall in January. The dry season affects the months from May to September, where the months of April and October mark the transition between the rainy - dry and dry - rainy periods, respectively (França et al. 2021). According to Liang et al. (2020), the average rainfall shows higher levels in the period from January to March and lower in the period from July to September.

The trade winds blow from the NE and SE, which predominate in the equatorial region and converge in the AICS, which changes throughout the year between August and September, further north, and between March and April near the Equator with a speed between 5 and 10 m.s<sup>-1</sup>, and a maximum between December and April. When added to the SE commercial wings (Rodrigues and Silva 2021; Lentini et al. 2021).



**Fig. 1** The inner continental shelf of Amapá (ICSA). The Varador channel separates the Maracá Island from the Atlantic coast of Amapá, R: River

### 3.2 Water and solid discharge from Amazon river

The Amazon River has a water flow of  $5.7 \times 10^{12} \text{ m}^3 \text{ year}^{-1}$ , with an average of  $200,000 \text{ m}^3 \text{ s}^{-1}$ , a maximum of  $220,000 \text{ m}^3 \text{ s}^{-1}$  (May) and a minimum of  $100,000 \text{ m}^3 \text{ s}^{-1}$  (November) (Gouveia et al. 2019; Liang et al. 2020). Water discharge from the Amazon River reaches its maximum in April - May along the north flow of the ICSA, and in June and July the flow contributes to the north equatorial countercurrent (Gouveia et al. 2019; Liang et al. 2020), in addition, the maximum flow in the North Channel reaches a volume of  $160,000 \text{ m}^3 \text{ s}^{-1}$ . Solid discharge from the Amazon River to the Amazon continental shelf is estimated at  $1.1$  to  $1.3 \times 10^9 \text{ ton} \cdot \text{year}^{-1}$  (Cunha et al. 2021).

### 3.3 Oceanographic conditions

In the region, the tide is semidiurnal, with a maximum and minimum height of 3.4, /0.2 m (Barra Norte), 5 m/0.3 m (Grande Curuá "igarapé") and 3.5/0.1 m (Santana port) (DHN 2024). On the other hand, on Maracá Island, the hyper tide reaches a maximum height of 11–12 m (DHN

2024). The ICSA is subject to the greater M2 component activity (12.42 h period) associated with the other components S2 (12 h) and N2 (12.66 h), which act on the sea level rise variation around 85% (Beardsley et al. 1995; Gurgel 2015; Gallo and Vinzon 2015). Tidal currents are characterized by two components, the coastal subtidal flow and the semidiurnal barotropic tidal flow. Tidal currents cause shear stress on the seafloor, participating in the process of sediment transport and granulometric distribution. The velocity of tidal currents reaches a maximum velocity of  $2 \text{ m} \cdot \text{s}^{-1}$  (spring) and a minimum of  $0.7 \text{ m} \cdot \text{s}^{-1}$  (neap) in the ICSA (Torres et al. 2018).

## 4 Methodology

### 4.1 Hydrodynamic model

According to Rosman (2021), the SisBaHiA hydrodynamic model fits into the Filtered in Space and Time (FIST) lineage and some of its characteristics confirm the importance and flexibility of the method. The numerical schemes of

the models are well established, which makes validity and acceptance more precise. The two-dimensional model (2D) has only the dimensions (x, y, t), and can be classified by two types of dimensions: (1) vertical (2DV) and (2) horizontal (2DH) (Rosman 2021).

For the analysis of the hydrodynamic circulation in a two-dimensional flow, the following aspects were taken into account: the average vertical velocities (U and V in the x and y directions) and the free surface level ( $\zeta$ ) according to the following equations (Rosman 2021):

Expression for the 2DH moment for vertically integrated flux in the y direction:

$$\begin{aligned} & \frac{\partial V}{\partial t} + U \frac{\partial V}{\partial x} + V \frac{\partial V}{\partial y} - 2\Phi \sin\theta U \\ & = -g \frac{\partial \zeta}{\partial y} + \frac{1}{\rho_0 H} \left( \frac{\partial (H\tau_{xy})}{\partial x} + \frac{\partial (H\tau_{yy})}{\partial y} \right) + \frac{1}{\rho_0 H} (\tau_y^s - \tau_y^B) \end{aligned} \quad (1)$$

Expression for momentum 2DH for vertically integrated flow in x direction:

$$\begin{aligned} & \frac{\partial U}{\partial t} + U \frac{\partial U}{\partial x} + V \frac{\partial U}{\partial y} - 2\Phi \sin\theta V \\ & = -g \frac{\partial \zeta}{\partial x} + \frac{1}{\rho_0 H} \left( \frac{\partial (H\tau_{xx})}{\partial x} + \frac{\partial (H\tau_{xy})}{\partial y} \right) + \frac{1}{\rho_0 H} (\tau_x^s - \tau_x^B) \end{aligned} \quad (2)$$

Continuity expression (volume) integrated along the vertical:

$$\frac{\partial \zeta}{\partial t} + \frac{\partial UH}{\partial x} + \frac{\partial VH}{\partial y} = 0 \quad (3)$$

Where:

- g – Represents the gravity acceleration;
- $\rho_0$  – Equals to specific mass of constant value;
- H – Spontaneous total depth;
- $\tau_{xx}, \tau_{xy}, \tau_{yy}$  – Represent the turbulent stresses in vertical;
- $\tau_x^s e \tau_y^s$  – Equivalent to frictional stresses on surface in respective x and y directions;
- $\tau_x^B e \tau_y^B$  – Equivalent to the frictional stress at bottom in respective x and y directions;
- $\Phi$  – Earth rotation angular speed on local coordinate system and  $\theta$  it's the latitude angle.

## 4.2 Input data for the hydrodynamic model

The application of the hydrodynamic model in SisBaHiA requires a set of input data (tidal elevation, bathymetry, bottom roughness, winds, maps and satellite images) to configure the project discretization. The ICSA mesh was created in SisBaHiA<sup>®</sup> after importing the base map and land and ocean contours, both adjusted in Surfer 23 (Table 1). The ICSA modeling domain was based on nautical charts from the Directorate of Hydrography and Navigation of the Brazilian Navy (DNH), with nautical chart no. 21,200 at a scale of 1:300,000 (3° 30') for the oceanic region, however, for the Atlantic coast of Amapá, the Topex altimetry program was used. At ICSA, computational modeling was used in the QuantunGis software to generate bathymetric data, which were interpolated and later compared with bathymetry data from the Topex altimetry program. The roughness parameters were adopted as recommended in SisBaHiA<sup>®</sup> (Rosman 2009). The tide data - harmonic constants and Variable Mean Level (Elevation) were extracted through a SisBaHiA<sup>®</sup> database (Rosman 2021) and, as for the wind data, they were acquired through periodic information from Copernicus Europe's eyes on Earth – ERA5, at single levels of peaks in the dry (October) and rainy (April) periods of the study area. In the Hydrodynamic Model (2DH), boundary conditions were imposed according to tidal current patterns based on the momentum of the water mass using software that participates in the modeling stages in SisBaHiA such as Surfer, Grapher, Google Earth Pro and Excel for data organization. The models produced virtually from the input data in SisBaHiA virtually represent the hydrodynamic behavior of the ICSA. Therefore, data on tide levels, currents and bathymetry play an important role in the model, as they influence the quality of the results. The discretization of the spatial domain with module 2DH was carried out using quadrangular finite elements with 9 nodes and triangular finite elements with 6 nodes connected to each other, where the average speed and surface elevation of each node in the domain are determined.

Tidal velocity and direction data were also used to identify responses to seasonal variations in hydrodynamics in the ICSA. To define the periods of spring and neap in the model, the April 2021 time series (30 days) was used. The bathymetric data were reduced by 0.5 m above the low mid-tide spring RL (MLWS). An elevation of 3.1 m above the NR (mean height from sea level – MS: mean sea level) was considered, referring to Guarás Island (0° 36' N – 57° 54.9'). The harmonic analysis was carried out using the SisBaHiA<sup>®</sup> Tide Analysis and Prediction Module, where three points were selected in the ICSA for the acquisition of tidal data for the calculation of the harmonic constants (Fig. 2).

**Table 1** Mesh data of square and triangular elements used in ICSA Amapá's Inner Continental Shelf

|                                |                                  |
|--------------------------------|----------------------------------|
| Elements numbers               | 309                              |
| Nodes numbers                  | 1363                             |
| Average distance between nodes | 1500 m                           |
| Mesh area                      | 2.049.349.185.155 m <sup>2</sup> |



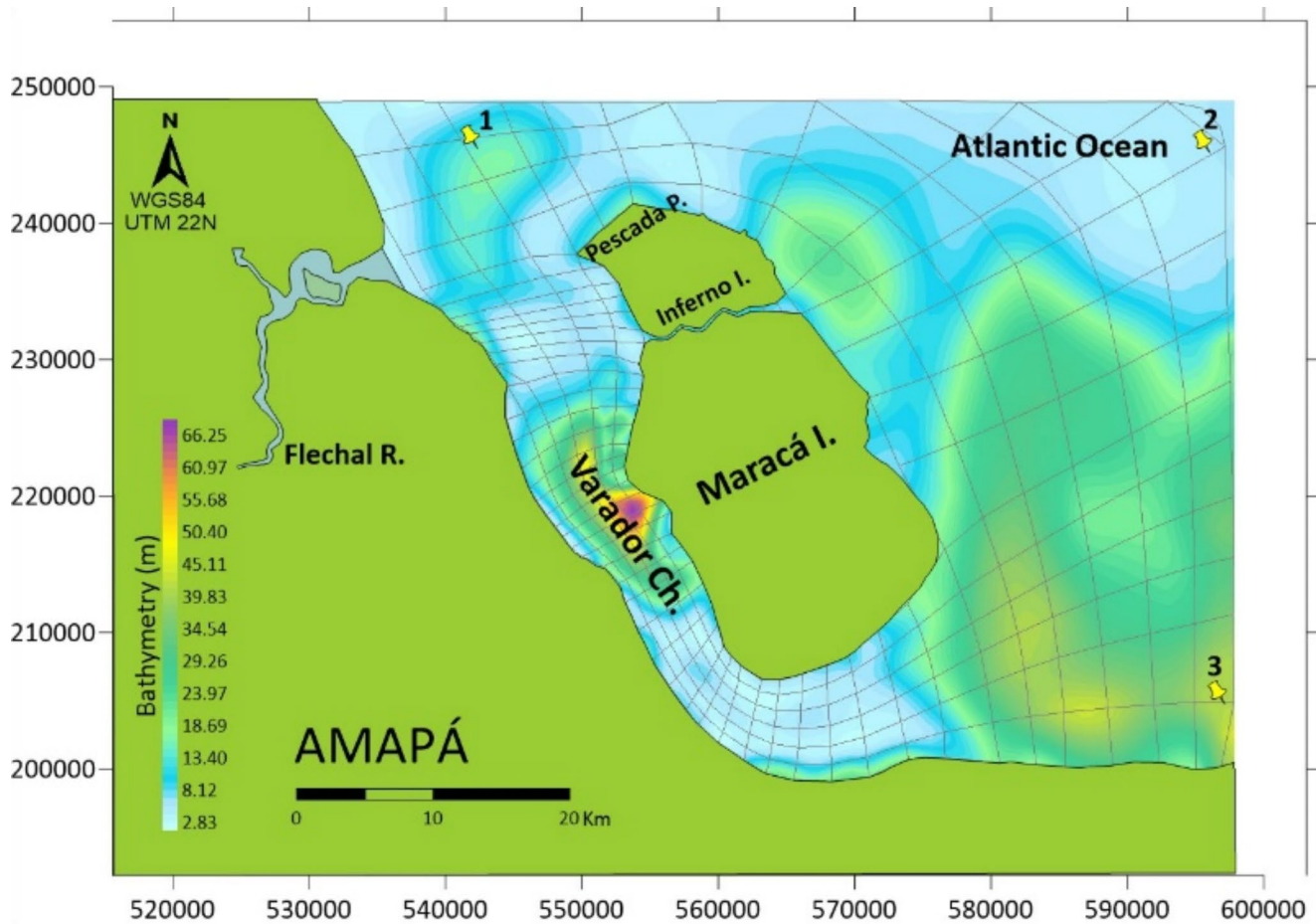


**Fig. 2** Discretization mesh and station location with harmonic constant data in ICSA, P: Point, I: Island, R: River, Ch: Channel, I: "Igarapé"; 1, 2 and 3 generic tide stations

In this way, we selected three stations (FES 1, FES 2 and FES 3) in the study area (Fig. 3) to acquire generic tidal data (Figs. 4 and 5) in ICSA to obtain information regarding harmonic constants, which were used in the development of the grid and modeling domain in the SisBaHia. 31 harmonic constants were used according to the FES database in the SisBaHia<sup>®</sup> tool tab.

Eight hydrodynamic simulations were generated during mid-flood, high tide, mid-ebb, low tide, both for spring and neap tides.

### 4.3 Energy density calculation

The energy density per square meter available from a tidal current kinetic energy is calculated according to the equation (Hagerman et al. 2006):

$$\left(\frac{P}{A}\right)_{water} = \frac{1}{2} \rho \cdot U^3 \text{ (W} \cdot \text{m}^{-2}\text{)} \tag{4}$$

Where:

“P” is equivalent to power, “A” is the transversal area of the flow intercepted by the device, “ $\rho$ ” is the water density in kilograms per cubic meter (1000 kg.m<sup>-3</sup> for fresh water and 1025 kg.m<sup>-3</sup> for sea water) and “U” is the tidal current velocity (m.s<sup>-1</sup>) This last variable changes predictably over the time and it’s directly related to depth and position.

## 5 Results

### 5.1 Model validation

To validate the model, a comparison was made between the real and modeled data, whose tidal height data were used as a parameter comparing the elevations generated in the simulations for the rainy period from 04/01/2021 to 04/30/2021 and at identified elevations (Fig. 4). The tide elevation curve resulting from the modeling generated a maximum elevation of 7.55 m and a minimum of 0.40 m for the second spring tide of the analyzed period, demonstrating values

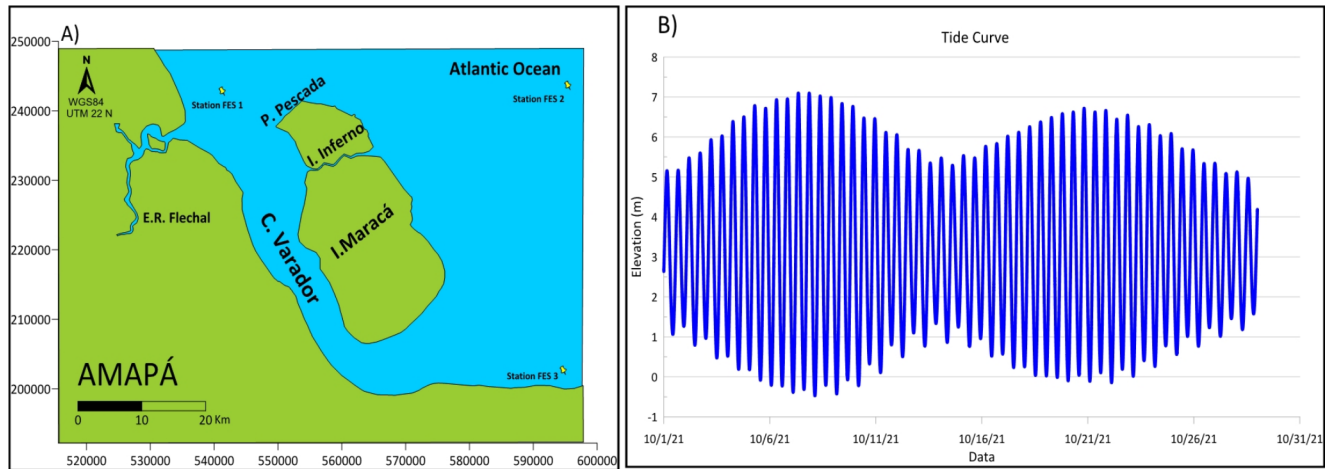


**Fig. 3** A) FES data station. B) Astronomical Tide – Station 1 FES in the dry period

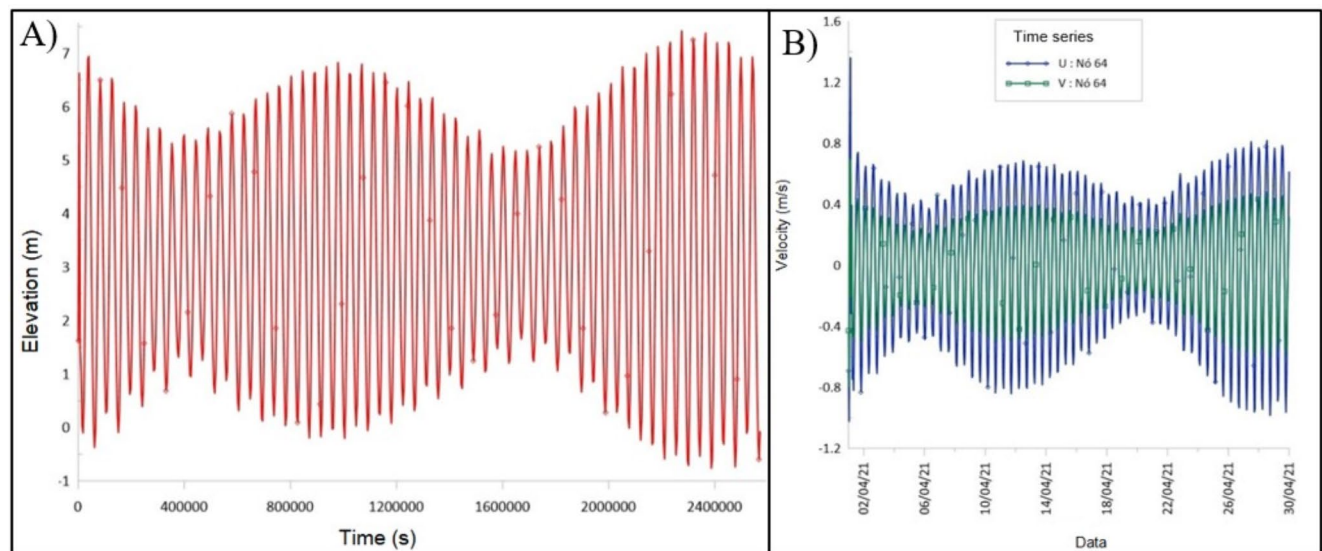


**Fig. 4** A) Tide raise curve generated by SisBaHiA for a period of 30 days, starting April 1, 2021. B) U (longitudinal velocity) and a V (transversal velocity) at node 64

close to the real one in comparison with the data from tide stations close to the ICSA.

To validate the values of tidal currents in the ICSA, Rosman's approach (2009) was used, in its site selection analysis for energy extraction from tidal currents in Brazil, to compare the results of the generated tidal currents, which presented a higher U velocity than the transversal V velocity, with a minimum U velocity of  $-1.053 \text{ m.s}^{-1}$  and a maximum of  $1.361 \text{ m.s}^{-1}$ , while the V velocity has a minimum of  $-0.793 \text{ m.s}^{-1}$  and a maximum of  $0.697 \text{ m.s}^{-1}$ .

The results for amplitude and tidal currents, as well as depths, were compared according to the approach of the AMASSSEDs (1990), the modeling of Fontes et al. (2008), Rosman (2009) and Molinas (2020). The study by Rosman

(2009) showed currents with a velocity of up to  $1.1 \text{ m.s}^{-1}$  in the ICSA (Table 2) during the flood period, where (present study), with reference to node 64.

Analyzing the results of the AMASSSEDs (1990) and the modeling obtained by Fontes et al. (2008) for the M2 tidal component from NW to SE along the Amapá coast (Table 3), it is observed that the results of the study model are within the validated parameters.

In addition to the comparison between the previous data, a statistical relationship was also made between the observed and modeled elevations. During the validation process, the difference (Table 4) was considered, which evaluates the difference between the simulated data and the

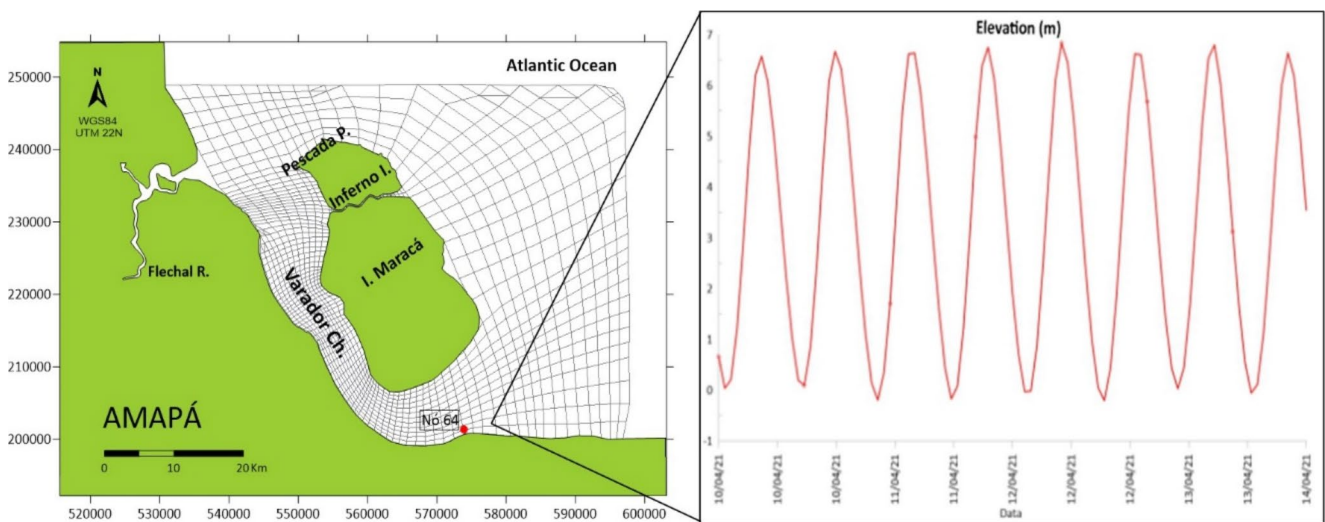


**Fig. 5** Tide rise in the lower section of the Varador channel: maximum of 6.8 m and minimum of -0.2 m for the first spring tide of the period and maximum of 7.55 m and minimum of 0.40 m for the second spring

tide of the analyzed period, P: Point, I: Island, R: River, Ch: Channel, I: "Igarapé"

**Table 2** Comparison of depths and tidal currents in the ICSA region

| Area | Rosmam (2009) |                              | Molinas (2020) |                              | Modeling (this paper) |                              |
|------|---------------|------------------------------|----------------|------------------------------|-----------------------|------------------------------|
| PCIA | Depth (m)     | Current (m.s <sup>-1</sup> ) | depth (m)      | Current (m.s <sup>-1</sup> ) | Depth (m)             | Current (m.s <sup>-1</sup> ) |
|      | 0–25          | -                            | 0–20           | 0,1–0,14                     | 0–24                  | 0–1.1                        |

**Table 3** Comparison of model results with reference to the tidal harmonic constant M2

| Area      | AMASSEDS (1990) |                              | Fontes; Fontes et al. (2008) |                              | Modeling (this paper) |                              |
|-----------|-----------------|------------------------------|------------------------------|------------------------------|-----------------------|------------------------------|
| I. Maracá | Amplitude (m)   | Current (m.s <sup>-1</sup> ) | Amplitude (m)                | Current (m.s <sup>-1</sup> ) | Amplitude (m)         | Current (m.s <sup>-1</sup> ) |
|           | 3,51            | 0,41                         | 3,00                         | 0,39                         | 2,94                  | 0,42                         |

**Table 4** Tide rise data for mid-tide neap and a difference between observed and modeled data

| Elevation (m) | Modeling (AMASSEDS (1990); Fontes et al. (2008)) | Simulation (this paper) | Difference |
|---------------|--|-------------------------|------------|
| Maximum       | 3,81   | 3,51                    | 0,17       |
| Minimum       | 3,65   | 3                       |            |
| Mean          | 3,46   | 3,25                    |            |

observed data. The result of the difference values for the first mid-tide neap were 0.17.

### 5.2 Hydrodynamic simulations

Verification of the results in the SisBaHiA<sup>®</sup> hydrodynamic model was provided in seconds, where, in all simulations, the spatial and temporal intervals were 3600 s and 1200 s, respectively, presenting 1 result every twenty minutes. From the first analysis of the high tide curve, an initial time

of 979,200 s was adopted for all simulations, with a final time of 2.570,400 s with 50 s elapsed.

The objective of the simulation is to analyze the hydrodynamic behavior in the ICSA during spring and neap tides and their intervals: mid-high tide, mid-low tide, high tide and low tide. The initial conditions of the 2DH model in SisBaHiA define aspects of the hydrodynamic circulation according to the initial time  $t_0$  for all domain nodes, generating free surface elevation values, as well as the U and V velocity components.

In the model, it is necessary to have the value of the elevation of the surface at instant 0, which is represented graphically and determined in the curves of the harmonic constants. The results obtained through the initial conditions of the 2DH model established the patterns of tidal currents according to the vector fields that represent the velocities of the x and y components of the water column, allowing the analysis of the average velocity, direction and intensity of tidal currents in the ICSA.

## 5.2.1 Spring tide

**5.2.1.1 Mid-flood tide (simulation 1)** At mid-flood tide, the greatest elevation amplitudes occur at the north and south ends of the Varador channel, respectively close to the Flechal river and Igarapé do Inferno (Maracá island) and, in the lower part, with small variations in elevation amplitudes during the flood. Elevation and tide inland ranged from 2,12 to 2,44 m but were between 2,64 and 2,72 m in most large part of the ICSEA (Fig. 6.a). The velocity modules generated for the U and V components vary between  $0.0 \text{ m.s}^{-1}$  and  $1,86 \text{ m.s}^{-1}$ . The largest tidal current velocity fields oscillate between  $1,09 \text{ m.s}^{-1}$  and  $1.53 \text{ m.s}^{-1}$ , in the upper part of the Varador channel. At this time, tidal currents have a speed of less than  $1.0 \text{ m.s}^{-1}$ , oscillating between  $0.44 \text{ m.s}^{-1}$  and  $0.98 \text{ m.s}^{-1}$  in most ICSEA.

**5.2.1.2 High tide (simulation 2)** At high tide (spring), there is a standardization of the tide rise in the ICSEA in several areas, with minimum tidal height, much higher than at the neap moment. In the outer part of the ICSEA the tide elevation was between 6.67 and 6.85 m with a gradual increase in the inner part of the Varador channel (6.88–7 m) and velocity between  $0 \text{ m.s}^{-1}$  and  $0.37 \text{ m.s}^{-1}$  near Ponta da Pescada (Fig. 6.b).

**5.2.1.3 Mid-ebb tide (simulation 3)** At mid-ebb tide, the tidal elevation remains high in the inner part of the Varador channel (2.46–2.62 m), with greater water flow throughout the entire length. At ICSEA, tidal elevation varied between 2.17 and 2.41 m on the outer part of Maracá Island. Also, tidal currents had the highest velocities ( $0.44 \text{ m.s}^{-1}$  to  $1.24 \text{ m.s}^{-1}$ ), near "Igarapé" do Inferno (Maracá Island) (Fig. 7.c).

**5.2.1.4 Low tide (simulation 4)** At low tide, the relative standardization of the tidal rise had a gradual increase up to the central part of the Varador channel (0.21–0.40 m), with small differences in the outer part of Maracá Island (0.2–0.17 m) and velocity from  $0 \text{ m.s}^{-1}$  to  $0.43 \text{ m.s}^{-1}$  (Fig. 7.d). The strongest tidal currents ( $1.31$ – $1.85 \text{ m.s}^{-1}$ ) occur in the narrowest stretch between the Atlantic coast of Amapá and Maracá Island, close to Cabo Norte.

## 5.2.2 Neap tide

**5.2.2.1 Mid-flood tide (Simulation 5)** At mid-flood tide, the tidal rise is between 2.84 and 2.94 m, towards the north

of Maracá Island, and between 2.66 and 2.91 m on the outer part of the ICSEA. The elevations for this period were close to those identified in the mid-tide simulation of spring and there is a movement of the water mass towards the outer part of the Maracá Island due to the ebb tide. The tidal currents had lower velocities in relation to the mid-ebb period of the spring, where the flow is more intense at the ends of the Varador channel (Ponta da Pescada/Maracá Island) and towards Cabo Norte (Fig. 7.a).

**5.2.2.2 Low tide (Simulation 6)** At low tide, there was little difference in relation to the elevation of the ebb tide in the neap, although in the Varador channel there was a reduction in elevation of 0.5 m, with low speeds of tidal currents, ranging from  $0 \text{ m.s}^{-1}$  to  $0.32 \text{ m.s}^{-1}$  in ICSEA. Outside the ICSEA, high tide ranged from 2.57 to 2.67 m with higher elevations near Cabo Norte (Fig. 7.b).

**5.2.2.3 Mid-flood tide (Simulation 7)** At mid-flood tide, elevations above 3 m were observed throughout the domain, as well as tidal current velocity between  $0 \text{ m.s}^{-1}$  and  $0.41 \text{ m.s}^{-1}$ . The highest elevation stretch (3.76–3.81 m) in the ICSEA occurred in the Varador channel near Cape Norte. However, the highest tidal current velocities ( $0.77 \text{ m.s}^{-1}$  to  $1 \text{ m.s}^{-1}$ ) were recorded near "Igarapé" do Inferno (Maracá Island) (Fig. 7.c).

**5.2.2.4 High tide (Simulation 8)** At high tide, the tide rise had low variation, with a maximum of 5.50 m in the central part of the Varador channel, lower in spring high tide. At ICSEA the tidal rise was 5.18–5.36 m in the outer part of the Maracá Island, however, the tidal velocity was  $0 \text{ m.s}^{-1}$  and  $0.12 \text{ m.s}^{-1}$  in the same area (Fig. 7.d).

## 5.3 Energetic density

In the northern and southern parts (Cabo Norte) of the Varador Channel, areas with tidal current fields were identified, with higher velocity in the ICSEA during the spring-neap cycle. Thus, the highest energy densities were measured in both periods (Table 5).

From the determination of the hydrodynamic simulations during the spring (1–4) and neap (5–8) in the ICSEA, a division of the hydrodynamic modeling domain was created and areas with velocities superior to  $1,0 \text{ m.s}^{-1}$ , favorable to energy extraction according to Fraenkel (2007). In simulation 2 (spring high tide), as well as in simulation 4 (spring low tide) there was no occurrence of tidal currents



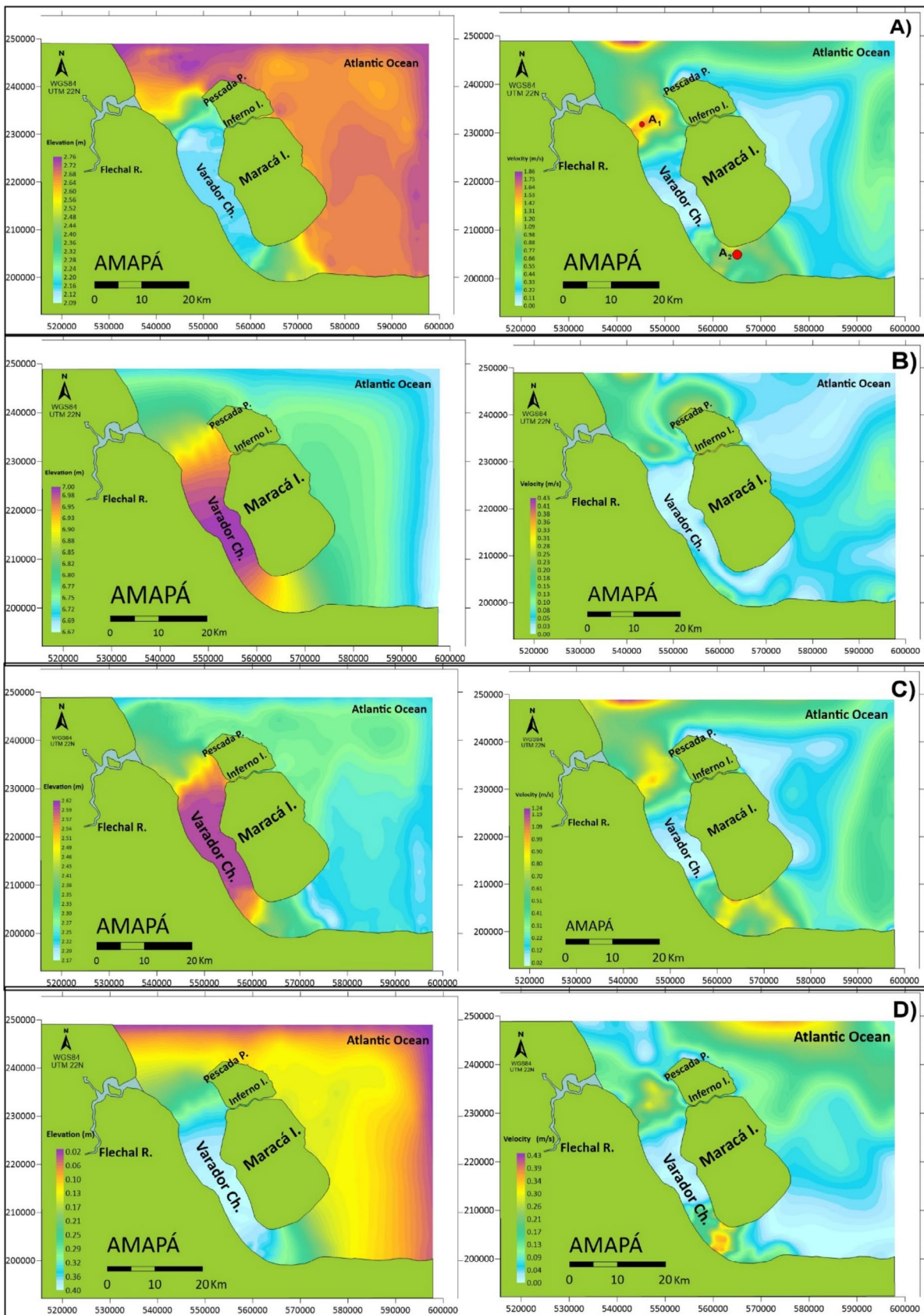


**Fig. 6** Spring tide - Elevation and tidal current standards at moments **A)** mid-flood tide. **B)** high tide. **C)** mid-ebb tide. **D)** low tide in ICSEA. A1 - Area A1, A2 - Area A2, P: Point, I: Island, R: River, Ch: Channel, I: "Igarapé"

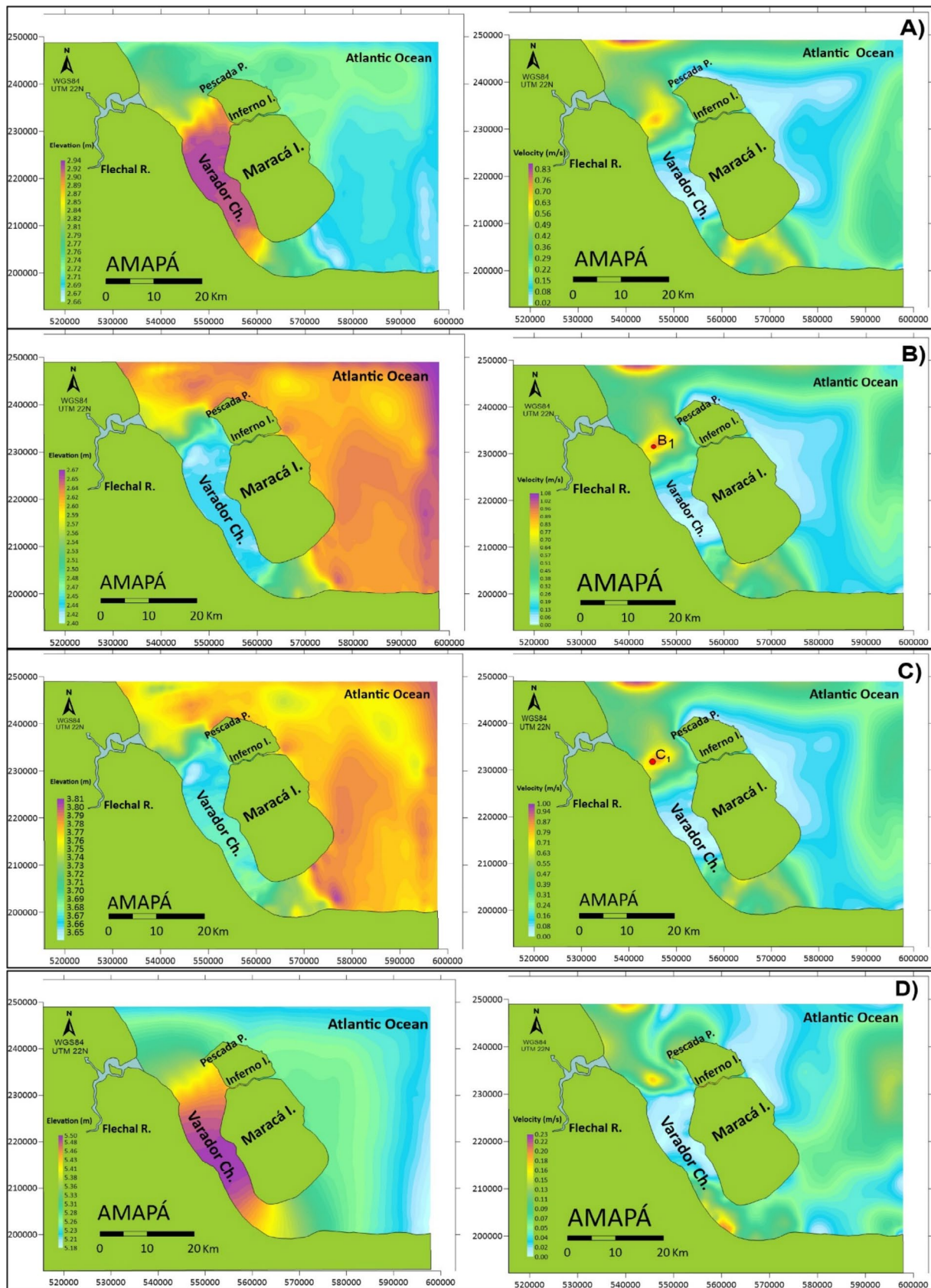


**Fig. 7** Neap – Elevation and tidal current standards at moments A) mid-ebb tide. B) Low tide. C) mid-flood tide. D) High tide. B1- Area B1, C1- Area C1, I: "Igarapé", P: Point, I: Island, R: River, Ch: Channel, I: "Igarapé"

**Table 5** Energy densities calculated in ICSA stretches during tidal simulations and their respective tidal current velocities

| Spring tide    |                 |                |                               |                        |                   |
|----------------|-----------------|----------------|-------------------------------|------------------------|-------------------|
| Area           | km <sup>2</sup> | Period         | Velocity (m.s <sup>-1</sup> ) | Total Gross Power (kW) | W.m <sup>-2</sup> |
| A <sub>1</sub> | 29,85           | Mid-flood tide | 1,53                          | 54.791,466             | 1.835,56          |
| A <sub>2</sub> | 18,37           | Mid-flood tide | 1,31                          | 21.164,996             | 1.152,15          |
| C <sub>1</sub> | 24,19           | Mid-ebb tide   | 1,14                          | 18.367,225             | 759,29            |
| C <sub>2</sub> | 27,27           | Mid-ebb tide   | 1,12                          | 19.635,218             | 720,03            |
| Neap tide      |                 |                |                               |                        |                   |
| B <sub>1</sub> | 18,90           | Low tide       | 1,08                          | 12.201,840             | 645,60            |
| C <sub>1</sub> | 17,49           | Mid-flood tide | 0,9                           | 6.534,438              | 373,61            |

with velocity above 1,00 m.s<sup>-1</sup>. For the neap period, simulations 6 (low tide) and 7 (mid-high tide) showed maximum tidal current velocity around 1,00 m.s<sup>-1</sup>. Simulation 8 (high tide) showed the lowest tidal cycle velocities (0,0 - m.s<sup>-1</sup> to 0,23 m.s<sup>-1</sup>).

The places with relevant power density occur in the Varador channel: the upper section with a total power density of 54.791,466 KW (mid-flood tide - currents of 1,53 m.s<sup>-1</sup>) and 18.367,225 KW (mid-ebb tide - currents 1,14 m.s<sup>-1</sup>), both during spring; and the lower section near Cabo Norte, with a total power density of 21.164,996 KW (mid-flood tide - currents of 1,31 m.s<sup>-1</sup>) and 19.635,218 KW (mid-ebb tide- currents of 1,12 m.s<sup>-1</sup>)(Table 5).

## 6 Discussion

### 6.1 SisBaHiA hydrodynamic model

Hydrodynamic models in homogeneous fluid indicate the pattern of currents in bodies of water with free surface, such as estuaries (Rosman 2021) and according to Cunha (2017), the properties of fluids can be conjectured through statistical methods for evaluating solutions analytical through numerical hydrodynamic models. SisBaHiA is considered an adequate tool to produce hydrodynamic simulations (Dalazen et al. 2020; França et al. 2021). The results of the hydrodynamic analysis provided a representation of the hydrodynamic circulation in the ICSA based on the tidal current velocities calculated by the model.

### 6.2 Energy density available in ICSA

According to the analysis of hydrodynamic simulations (8) developed at ICSA during the spring and neap moments, fields of tidal currents were identified, with velocity greater than 1 m.s<sup>-1</sup> (Table 5):

### 6.2.1 Spring tide

The highest speeds occur in the rising mid-tide and in the ebbing mid-tide.

- (1) In the upper section of the Varador channel (16–18 m depth), at mid-flood tide the velocity reached 1,53 m.s<sup>-1</sup> and the corresponding energy density of 1.835,56 W.m<sup>-2</sup>;
- (2) Near the lower section of the Varador channel (4–8 m depth) south of Maracá Island, a field of tidal currents with a velocity of 1,31 m.s<sup>-1</sup> was identified at mid-flood tide, and the corresponding incident power is 1.152,15 W.m<sup>-2</sup>;
- (3) In upper stretch of the Varador channel (Fig. 7.c) during mid-ebb tide, a tidal current velocity field of 1,14 m.s<sup>-1</sup> was identified and the energy density was 759,29 W.m<sup>-2</sup>;
- (4) In the lower section of the Varador channel (Fig. 7.c), during the mid-ebb tide, a tidal current field reached a velocity of 1,12 m.s<sup>-1</sup> and corresponds to an incident power of 720,03 W.m<sup>-2</sup>.

### 6.2.2 Neap tide

- (1) In the Varador channel, the tidal current field had a lower velocity compared to the spring tidal moment. At low tide, the tidal current field reached a velocity of 1,08 m.s<sup>-1</sup>, with an energy density of 645,60 W.m<sup>-2</sup>;
- (2) In the Varador channel (Fig. 7.c) and during mid-flood tide, the current field reaches a speed of 0,9 m.s<sup>-1</sup> and the corresponding energy density of 373,61 W.m<sup>-2</sup>;

During the spring tide, the ICSA exhibited a total area of 99,680,000 m<sup>2</sup> with an energy density of 113,958,905 kW, however, in the neap tide, the total area was 36,390,000 m<sup>2</sup> with an energy density of 18,736,278.9 kW.

## 6.3 Comparison with other regions of Brazil and world

The tidal regime has an important advantage in terms of predictability of its behavior, where the speed of the currents at high or low tides to the detriment of its semidiurnal regime and seasonality (rainy and dry periods) determine the places of considerable energy density. During the spring tidal cycle, the flow follows towards the coast with a velocity variation of 1.09 to 1,53 m.s<sup>-1</sup> in narrow segments of the ICSA, where in most of the domain the tidal currents oscillate between 0.44 and 0.98 m.s<sup>-1</sup>, the velocity varies from



zero (low tide) to a maximum and then decelerates at high tide. During ebb tide, the flow direction changes towards the ocean and accelerates again according to the cyclic behavior of the tides.

According to Rosman (2009), a considerable area of the ICSA exhibited tidal current velocity below  $1,1 \text{ m}\cdot\text{s}^{-1}$  most of the time during a simulation period of 2 months. The modeling area near the Varador channel demonstrated in 50% of the time minimum tidal current velocities lower than  $1,1 \text{ m}\cdot\text{s}^{-1}$ .

Assuming the minimum parameters for hydrokinetics (Fraenkel 2007; Lim and Koh 2010; Myers and Bahaj 2012), some stretches of the Varador channel present energetic potential in both periods, spring (i) and neap (ii) (Table 2): (i) Areas A<sub>1</sub> with  $1.835,56 \text{ W}\cdot\text{m}^{-2}$  and A<sub>2</sub> with  $1.152,15 \text{ W}\cdot\text{m}^{-2}$  in mid-flood tide (Fig. 6.a) and areas C<sub>1</sub> with  $759,29 \text{ W}\cdot\text{m}^{-2}$  and C<sub>2</sub> with  $720,03 \text{ W}\cdot\text{m}^{-2}$  (Fig. 6.c) during mid-ebb tide; (ii) Areas B<sub>1</sub> with  $645,60 \text{ W}\cdot\text{m}^{-2}$  at low tide and C<sub>1</sub> with  $373,61 \text{ W}\cdot\text{m}^{-2}$  (Fig. 7.c) at mid-flood tide also showed energy potential.

The average energy density in Chacao Channel (Chile) is greater than  $5 \text{ kWm}^{-2}$  (Guerra et al. 2017). In Todos os Santos Bay (Brazil), the average energy density is  $400 \text{ Wm}^{-2}$  and reaches a peak of  $2,5 \text{ kWm}^{-2}$  (Marta-Almeida et al. 2017; Vogel et al. 2019). In São Marcos Bay (Maranhão / Brazil), the energy density is between  $1,5$  and  $7,5 \text{ kWm}^{-2}$  (González-Gorbeña et al. 2015). In Yangtze River estuary (China), the maximum energy density can exceed  $10 \text{ kWm}^{-2}$  and in the Chengshan cape, located in the most eastern part of Weihai (Shandong province/China), the average energy density is  $2 \text{ kWm}^{-2}$  (Liu et al. 2021).

According to the results of this article, locations with relevant energy density were identified when compared to other estuaries in other parts of the world, which allows the hypothesis of installing turbines to generate electricity. Concomitantly with the development of new technologies for low-speed turbines (Yosry et al. 2021), the indicated sections with considerable energy density become economically exploitable according to the areas of energy potential and current speeds. Some sites can be compared to those identified by Czizewski et al. (2020); Liu et al. (2021).

Estuaries have many social, physical aspects that must be considered before introducing tidal energy devices and are habitat and breeding grounds for many marine species [McLusky and Elliot 2004]. On the other hand, estuaries provide environmental services and provide recreational and economic activities to riverside communities. The tidal currents in ICSA, with maximum velocities of  $1.53 \text{ m}\cdot\text{s}^{-1}$ , occur in the narrowest part of the Varador channel (Table 5), and where the bottoms are covered by fine sediments from the Amazon River, transported towards the north, by water discharge and macro tidal currents (Tenorio-Fernandez et al.

2019). Environmental data (water discharge of  $200,000 \text{ m}^3 \text{ s}^{-1}$ /Liang et al. 2020; solid discharge of  $160,000 \text{ m}^3 \text{ s}^{-1}$ /Cunha et al. 2021; hyper tide, with maximum height of  $11\text{--}12 \text{ m/DHN}$  2024; currents tide of  $1.53 \text{ m}\cdot\text{s}^{-1}$  and suspended material of  $700 \text{ mg}\cdot\text{L}^{-1}$  (April) and  $200 \text{ mg}\cdot\text{L}^{-1}$  (May)/Gensac et al. 2016) are relevant for the selection of sites for exploitation energy from tidal currents (Ross et al. 2021). Taking into account these environmental conditions in the Varador channel, an anchored hydrokinetic turbine is suggested to take advantage of tidal currents. Understanding the changes caused to the environment by the installation of tidal turbine technology involves both assessing the variation in energy density by determining the ideal location for applying the techniques and assessing the tidal currents (hydrodynamics) and suspended sediment concentration (SSC) in the estuary (Ross et al. 2021). The ecosystem and human populations determine the layout and location of tidal turbines to the detriment of the hydrodynamic impacts and sediment transport influenced by the implementation of tidal current energy extraction techniques.

The currents observed in this study indicate attractive energy densities for power generation, promoting the development of riverside communities and the production of green hydrogen in vast uninhabited areas. Given the region's morphological characteristics and the temperature, salinity, and turbidity of equatorial waters, turbines should be designed for these conditions to achieve optimal efficiency. Several recent studies report specific turbines for large Brazilian rivers and estuaries. For example, Gemaque et al. (2022), Rezek et al. (2023) and Cosme et al. (2023) report significant efficiency gains using diffuser turbines and other specific modifications.

## 7 Conclusion

The application of the Base System of Environmental Hydrodynamics (SisBaHiA) proved to be satisfactory for the development of hydrodynamic simulations (8), which allowed the identification of high tide current fields. Finally, the application of the energy density calculation pointed out the energy potential of several areas of the ICSA. The study area presents complexity for data entry in the software, however, the program proved to be efficient with results consistent with the real data. Through the hydrodynamic simulations carried out, it was verified that the minimum velocities of the tidal currents in the ICSA, occur only in the periods of flooding half-tide and ebb tide (spring), where they presented velocities between  $1,12 \text{ m}\cdot\text{s}^{-1}$  and  $1,53 \text{ m}\cdot\text{s}^{-1}$  at the ends of the Varador channel.

During high and low tides of the spring, tidal currents with velocities between  $0,16 \text{ m}\cdot\text{s}^{-1}$  and  $0\text{--}0,43 \text{ m}\cdot\text{s}^{-1}$ ,



respectively, over a large part of the domain, consistent with the movement of currents according to the summation periods. The tidal elevation curve resulting from the modeling generated a maximum elevation of 7,55 m and a minimum of 0,40 m for the second spring tide of the analyzed period, demonstrating values close to the real one in comparison with the data from the tide stations near the ICSA. Data from tidal velocity fields identified in hydrodynamic simulations, close to the upper and lower part of the Strait of Maracá Island, point to areas with greater energy potential compared to other ICSA locations. The velocities of tidal currents produced by the model proved to be adequate under the hydrodynamic aspects resulting from tidal cycles and geomorphological characteristics, where there are stretches with available energy potential. The unique characteristics of this Amazonian region provide a valuable case for the development of renewable energy technologies tailored to its environmental conditions, highlighting the potential for sustainable energy production as an alternative to offshore oil exploration. This approach not only addressed energy needs but also aligns with environmental conservation efforts, supporting both local and global sustainability goals.

**Author contributions** ERM (GEMC/master’s dissertation director) has been doing systematic research in Amazonian estuaries and designed the study in this geographical area. RWQF developed his dissertation. ORS participated in the discussion and all the authors contributed to the revision of the manuscript until its submission.

**Funding** The National Institute of Ocean Energy Science and Technology (INEOF/CNPQ), funded this research through the grant (Master’s Scholarship) from the Coordination for the Improvement of Higher Education Personnel - Brazil (CAPES) - Finance Code 001”. The Coastal and Marine Studies Group (GEMC/CNPQ) / Federal University of Pará - UFPA provided the laboratory and all the computer facilities for the research, within the scope of the Postgraduate Program in Naval Engineering (Institute of Technology/UFPA).

**Data availability** The hydrodynamic simulations were generated during spring and neap tides and their intervals: ½ high tide, ½ low tide, high tide and low tide. The 2DH model from the SisBaHiA software (Rosman 2009) was used. The energy density per square meter available from a tidal current kinetic energy is calculated according to the equation (Hagerman et al. 2006).

## Declarations

**Ethical approval** Not applicable.

**Consent to participate** Not applicable.

**Consent for publication** Not applicable.

**Conflict of interest** The authors declare no competing interests.

## References

- AMASSEDS (1990) an interdisciplinary investigation of a complex coastal environment. *Oceanography*, 4 (1): 3–7. <http://www.jstor.org/stable/43924555> AmasSeds Research Group Accessed 12th June 2023
- Azevedo TNA, El-Robrini M, Saavedra OR Assessment of tidal current potential in the Pará River Estuary (Amazon Region – Brazil), Cleaner Energy Systems 1–24., Candela J, Limeburner R, Geyer WR, Lentz SJ, Belmiro MC, Cacchione D, Carneiro N (2023) The M2 tide on the Amazon shelf: Journal of Geophysical Research 100: 2283–2319. <https://doi.org/10.1029/94JC01688>
- BNH - Brazilian Navy Hydrography Center. <https://www.marinha.mil.br/chm/dados-do-segnav/cartas-raster>. Accessed 19 Aug 2024
- Carneiro GL, Penteado Neto RA (2022) Avaliação De um sistema de tomada de força hidráulico para conversão de energia ondomotriz. *Conjecturas* 22(2):510–524. <https://doi.org/10.10100/CONJ-W01-001>
- Castello X, Estefen SF, Soares CR (2020) Os oceanos: os desafios para geração de energia sustentável. In: Lana, P. C.; Castello, J. P. (org.). *Fronteiras do conhecimento em ciências do mar*. Rio Grande: Ed. da FURG 158–180. ISBN: 978-65-5754-019-0
- Centro de Hidrografia da Marinha do Brasil (2024) <https://www.marinha.mil.br/chm/dados-do-segnav/cartas-raster>. Accessed in 1th
- Chowdhury MS, Rahman KS, Selvanathan VMS, Nuthammachot N, Suklueng M, Mostafaeipour A, Habib A, Akhtaruzzaman MD, Amin N, Techato K (2021) Current trends and prospects of tidal energy technology. *Environ Dev Sustain* 23:8179–8194. <https://doi.org/10.1007/s10668-020-01013-4>
- Cosme Diego LD, Veras R, Camacho Ramiro GR, Saavedra OR, Torres A, Andrade M (2023) Modeling and assessing the potential of the Boqueirão Channel for Tidal Exploration. *Renewable Energy* 1:119468. <https://doi.org/10.1016/j.renene.2023.119468>
- Cunha JRC (2017) Modelagem (Bidimensional – 2DH) Hidrodinâmica aplicada no estuário do rio Guamá (Estado do Pará/Brasil). Master’s thesis in Naval Engineering - Postgraduate Program in Naval Engineering, Institute of Technology, Federal University of (Brazil)
- Cunha C, de L da N, Scudelari AC, Sant’Ana D, de Luz O, Pinheiro TEB (2021) M. K. da R Effects on circulation and water renewal due to the variations in the river flow and the wind in a Brazilian estuary lagoon complex. *Revista Ambiente and Água* 16 (2): 1–18. <https://doi.org/10.4136/ambi-agua.2600>
- Czizewski A, Pimenta FM, Saavedra OR (2020) Numerical modeling of Maranhão Gulf tidal circulation and power density distribution. *Ocean Dyn* 70:667–682. <https://doi.org/10.1007/s10236-020-01354-8>
- Dalazen JP, Cunha C, da N de L, Almeida RC de (2020) Determinação das taxas de renovação das águas no complexo estuarino de Paranaguá. *Eng Sanit Ambient* 25(6):887–899. <https://doi.org/10.1590/S1413-4152202020180019>
- de França JMB, Neto JC, Neto IEL, Paulino WD, de Souza Filho F (2021) Simulação Da compartimentação em reservatório no semiárido brasileiro uso da modelagem hidrodinâmica como ferramenta de gestão. *Revista DAE*. São Paulo 69(231):41–53. <https://doi.org/10.36659/dae.2021.045>
- de Lima RF, Oliveira-Aparecido LE, Lorençone JA, Lorençone PA, Moraes JR da, de Meneses SC (2021) Climate scenarios and your changes in the life zone for Brazil. *Research Square* 1–25. <https://doi.org/10.21203/rs.3.rs-643200/v1>
- Dubreuil V, Fante KP, Planchon O, Sanánna Neto JL (2018) *Confins* 37:1–22. <https://doi.org/10.4000/confins.15738>. Os tipos de climas anuais no Brasil: uma aplicação da classificação de Köppen de 1961 a 2015

- Fontes RFC, Castro BM, Beardsley RC (2008) Numerical study of circulation on the inner Amazon Shelf. *Ocean Dyn* 58:187–198. <https://doi.org/10.1007/s10236-008-0139-4>
- Fraenkel PL (2007) Marine current turbines: pioneering the development of marine kinetic energy converters. *Proc Institution Mech Eng Part A: J Power Energy* 221(2):159–169. <https://doi.org/10.1243/09576509JPE307>
- Gallo MN, Vinzon SB (2015) Estudo numérico do escoamento em planícies de marés do canal norte (estuário do rio Amazonas). *RIBAGUA - Revista Iberoamericana Del Agua* 2:38–50. <https://doi.org/10.1016/j.riba.2015.04.002>
- Gemaque ML, Vaz JRP, Saavedra OR (2022) Optimization of Hydrokinetic swept blades. *Sustainability* 14:13968. <https://doi.org/10.3390/su142113968>
- Gensac E, Martinez JM, Vantrepotte V, Anthony EJ (2016) Seasonal and inter-annual dynamics of suspended sediment at the mouth of the Amazon river: The role of continental and oceanic forcing, and implications for coastal geomorphology and mud bank formation. *Cont Shelf Res* 118:49–62. <https://doi.org/10.1016/j.csr.2016.02.009>
- González-Gorbeña E, Rosman PCC, Qassim RY (2015) Assessment of the tidal current energy resource in São Marcos Bay, Brazil. *J Ocean Eng Mar Energy* 1:421–433. <https://doi.org/10.1007/s40722-015-0031-5>
- Gouveia NA, Gherardi DFM, Aragão LEOC (2019) The role of the Amazon River plume on the intensification of the hydrological cycle. *Geophys Res Lett* 46:12221–12239. <https://doi.org/10.1029/2019GL084302>
- Guerra M, Cienfuegos R, Thomson J, Suarez L (2017) Tidal energy resource characterization in Chacao Channel, Chile. *Int J Mar Energy* 20:1–16. <https://doi.org/10.1016/j.ijome.2017.11.002>
- Gurgel ARC (2015) Ressonância da onda de Maré na Plataforma Continental Amazônica. Master's thesis in Applied Physics - Postgraduate Program in Applied Physics, Federal Rural University of Pernambuco (Brazil)
- Hagerman G, Polagye B, Bedard R, Previsic M (2006) Methodology for estimating tidal current energy resources and power production by tidal in-stream energy conversion (TISEC) devices, EPRI North American tidal in stream power feasibility demonstration project. [https://diving-rov-specialists.com/index\\_html\\_files/os\\_24-tidal-current-energy-resources](https://diving-rov-specialists.com/index_html_files/os_24-tidal-current-energy-resources). Accessed 19th November 2023
- Instituto Nacional de Meteorologia - INMET Prognóstico de Precipitação (2024) <https://portal.inmet.gov.br/>
- Instituto de Pesquisa Econômica Aplicada - IPEA Energia acessível e limpa (2023) Disponível em: <https://www.ipea.gov.br/ods/ods7>. Accessed 20th
- Lentini CAD, Silva M, Veleza DRA, Araujo M, Cintra M, Varona HL, Teixeira CEP, Costa LVB, Mendonça LFF, Araujo J (2021) Oceanografia física do Atlântico tropical: processos hidrotermodinâmicos. *Ciências do Mar: Dos Oceanos do Mundo Ao Nordeste do Brasil* 76–97. <https://doi.org/10.5281/zenodo.8341727>
- Liang YC, Lo MH, Lan CW, Seo H, Ummerhofer CC, Yeager S, Wu RJ, Steffen JD (2020) Amplified seasonal cycle in hydroclimate over the Amazon river basin and its plume region. *Nat Commun* 11(1):4390. <https://doi.org/10.1038/s41467-020-18187-0>
- Lim YS, Koh SL (2010) Analytical assessments on the potential of harnessing tidal currents for electricity generation in Malaysia. *Renew Energ* 35:1024–1032. <https://doi.org/10.1016/j.renene.2009.10.016>
- Liu X, Chen Z, Si Y, Qian P, Wu H, Cui L, Zhang D (2021) A review of tidal current energy resource assessment in China. *Renew Sustain Energy Rev* 145:1–20. <https://doi.org/10.1016/j.rser.2021.111012>
- Marta-Almeida M (2022) Ocean modelling in Brazil, a quick overview. *Arquivo De Ciências do Mar. Fortaleza* 55:338–344. <https://doi.org/10.32360/78208>
- Marta-Almeida M, Cirano M, Soares CG, Lessa GC (2017) A numerical tidal stream energy assessment study for Baía De Todos Os Santos, Brazil. *Renewable Energy* 107:271–287. <https://doi.org/10.1016/j.renene.2017.01.047>
- Molinas E, Carneiro JC, Vinzon S (2020) Internal tides as a major process in Amazon continental shelf fine sediment transport. *Mar Geol* 430:1–26. <https://doi.org/10.1016/j.margeo.2020.106360>
- Myers LE, Bahaj AS (2012) An experimental investigation simulating flow effects in first generation marine current energy converter arrays. *Renew Energy* 37(1):28–36. <https://doi.org/10.1016/j.renene.2011.03.043>
- Neto PBL, Saavedra OR, De Souza LAR (2017) Analysis of a tidal Power Plant in the Estuary of Bacanga in Brazil taking into account the current conditions and constraints. *IEEE Trans Sustain Energy* 8(3):1187–1194. <https://doi.org/10.1109/TSTE.2017.2666719>
- Nittrouer CA, DeMaster DJ, Kuehl SA, Figueiredo AG, Sternberg RW, Faria LEC, Silveira OM, Allison MA, Kineke GC, Ogsston AS, Souza Filho PWM, Asp NE, Nowacki DJ, Fricke AT (2020) Amazon sediment transport and accumulation along the continuum of mixed fluvial and marine processes. *Annual Rev Mar Sci* 13(1):501–536. <https://www.annualreviews.org/content/journals/10.1146/annurev-marine-010816-060457>
- Oliveira CHC, Barros MLC, Branco DAC, Soria R, Rosman PCC (2021) Evaluation of the hydraulic potential with hydrokinetic turbines for isolated systems in locations of the Amazon region. *Sustain Energy Technol Assess* 45:1–22. <https://doi.org/10.1016/j.seta.2021.101079>
- Oliveira L, Santos IFS, Schmidt NL, Filho GLT, Camacho RGR, Barros RM (2021b) Economic feasibility study of ocean wave electricity generation in Brazil. *Renewable Energy* 178:1279–1290. <https://doi.org/10.1016/j.renene.2021.07.009>
- Pereira TJ, Castellões PV, Netto SA (2022) Amazon River discharge impacts deep-sea meiofauna. *Limnol Oceanogr* 67(10):2190–2203. <https://doi.org/10.1002/lno.12197>
- Rezek TJ, Camacho Ramiro GR, Manzaneres-Filho N (2023) A novel methodology for the design of diffuser-augmented hydrokinetic rotors. *Renewable Energy* 210:524–539. <https://doi.org/10.1016/j.renene.2023.04.070>
- Ridgill M, Neil SP, Lewis MJ, Robins PE, Patil SD (2021) Global riverine theoretical hydrokinetic resource assessment. *Renewable Energy* 174:654–665. <https://doi.org/10.1016/j.renene.2021.04.109>
- Rodrigues MRC, OM da Silva Jr (2021) Panorama Geral Da Zona Costeira do Estado do Amapá. *Revista Brasileira De Geografia Física* 14(3):1664–1674. <https://doi.org/10.26848/rbgf.v14.3.p1654-1674>
- Rosman PCC (2009) Analyses of the effects of turbine array densities in the tidal currents in São Marcos Bay-MA-Technical Report in project Selecting sites for tidal current power extraction in Brazil, Fundação Coppetec, PENO11297
- Rosman PCC (2021) Referência Técnica do SisBaHiA-Sistema Base de Hidrodinâmica Ambiental, Programa COPPE. Engenharia Oceânica: área de engenharia costeira e oceanográfica. UFRJ/Brasil 11:1–426
- Ross L, Sottolichio A, Huybrechts N, Brunet P (2021) Tidal turbines in the estuarine environment: from identifying optimal location to environmental impact. *Renewable Energy* 169. <https://doi.org/10.1016/j.renene.2021.01.039>
- Santos IFS, Camacho RGR, Filho GLT, Botan ACB, Vinent BA (2019) Energy potential and economic analysis of hydrokinetic turbines implementation in rivers: an approach using numerical predictions (CFD) and experimental data. *Renewable Energy* 143:648–662. <https://doi.org/10.1016/j.renene.2019.05.018>

- Sood M, Singal SK (2022) Development of statistical relationship for the potential assessment of hydrokinetic energy. *Ocean Eng* 266:1–20. <https://doi.org/10.1016/j.oceaneng.2022.112140>
- Tenorio-Fernandez, Zavala-Hidalgo J, Olvera-Prado ER (2019) Seasonal variations of river and tidal flow interactions in a tropical estuarine system, *Continental Shelf Research* v. 188:1–10. <https://doi.org/10.1016/j.csr.2019.103965>
- Thiébot J, Coles DS, Guillou BA-C, Neill N, Guillou S, Piggott S M (2020) Numerical modelling of hydrodynamics and tidal energy extraction in the Alderney race: a review. *Phil Trans R Soc* 378:1–30. <https://doi.org/10.1098/rsta.2019.0498>
- Torres A, El Robrini M, Costa WJP (2018) Erosão e progradação do litoral do Amapá. 2015. E – book. 12 – 40p. in: *Progradação do Litoral Brasileiro*, Muehe D (Org.) MMA. Brasília
- Vogel CR, Taira DT, Carmo BS (2019) Perspectivas para a energia do fluxo das marés no Reino Unido E na América do sul: uma revisão Dos desafios e oportunidades. *Politécnica* 2:97–109. <https://doi.org/10.1007/s41050-019-00017-y>
- Yosry AG, Fernández-Jiménez A, Álvarez-Álvarez E, Marigorta EB (2021) Design and characterization of a vertical-axis micro tidal turbine for low velocity scenarios. *Energy Conv Manag* 21(62):1–9. <https://doi.org/10.1016/j.enconman.2021.114144>

**Publisher's Note** Springer Nature remains neutral with regard to jurisdictional claims in published maps and institutional affiliations.

Springer Nature or its licensor (e.g. a society or other partner) holds exclusive rights to this article under a publishing agreement with the author(s) or other rightsholder(s); author self-archiving of the accepted manuscript version of this article is solely governed by the terms of such publishing agreement and applicable law.